# Electroweak baryogenesis, dark matter, and dark *CP* symmetry

Jinghong Ma, Jie Wang, and Lei Wang*

*Department of Physics, Yantai University, Yantai 264005, People's Republic of China*

(Received 14 November 2023; accepted 21 March 2024; published 15 April 2024)

With the motivation of explaining the dark matter and achieving the electroweak baryogenesis via the spontaneous *CP* violation at high temperature, we propose a complex singlet scalar ($S = \frac{\chi + i\eta_s}{\sqrt{2}}$) extension of the two-Higgs-doublet model respecting a discrete dark *CP* symmetry: $S \to -S^*$. The dark *CP* symmetry guarantees $\chi$ to be a dark matter candidate on one hand and on the other hand allows $\eta_s$ to have mixings with the pseudoscalars of the Higgs doublet fields, which play key roles in generating the *CP* violation sources needed by the electroweak baryogenesis at high temperature. The Universe undergoes multistep phase transitions, including a strongly first-order electroweak phase transition during which the baryon number is produced. At the present temperature, the observed vacuum is produced and the *CP* symmetry is restored so that the stringent electric dipole moment experimental bounds are satisfied. Considering relevant constraints, we study the simple scenario of $m_\chi$ around the Higgs resonance region, and find that the dark matter relic abundance and the baryon asymmetry can be simultaneously explained. Finally, we briefly discuss the gravitational wave signatures at future space-based detectors and the LHC signatures.

DOI: 10.1103/PhysRevD.109.075024

## I. INTRODUCTION

The baryon asymmetry of the Universe (BAU) presents one of the major quests for particle cosmology. By the observation based on the big bang nucleosynthesis, the BAU is [1]

$$Y_B \equiv \rho_B/s = (8.2\text{–}9.2) \times 10^{-11}, \tag{1}$$

where $\rho_B$ is the baryon number density and $s$ is the entropy density. Three necessary Sakharov conditions have to be fulfilled for a dynamical generation of BAU: baryon number changing interactions, nonconservation of $C$ and $CP$, and departure from thermal equilibrium [2]. The electroweak baryogenesis (EWBG) [3,4] provides a promising and attractive mechanism of explaining the BAU since it is testable at the energy frontier by the LHC and at the precision frontier by the electric dipole moment (EDM) experiments. To realize the EWBG, one needs extend the SM to produce sufficient large *CP* violation and a strongly first-order electroweak phase transition (EWPT), such as the singlet extension of SM (see, e.g., [5–19]) and the two-Higgs-doublet model (2HDM) (see, e.g., [20–38]).

The negative results in the EDM searches for electrons impose stringent constraints on the explicit *CP* violation interactions in the scalar couplings and Yukawa couplings [39]. There are some cancellation mechanisms of *CP* violation effects in the EDM, which can relax the tension between the EWBG and the EDM data [36,37,40–45]. Even with the cancellation, there are several *CP* observables of radiative $B$ meson decays that still provide stringent constraints, such as the asymmetry of the *CP* asymmetry of inclusive $B \to X_s\gamma$ decay [42,44], Alternatively, a finite temperature spontaneous *CP* violation mechanism is naturally compatible with the EDM data, where the *CP* symmetry is spontaneously broken at the high temperature and it is recovered at the present temperature. The novel mechanism was achieved in the singlet scalar extension of the SM [13,14] in which a high dimension effective operator needs to be added, and the singlet pseudoscalar extension of 2HDM [46,47].

In addition to the BAU, the dark matter (DM) is one of the longstanding questions of particle physics and cosmology. In this paper, we propose a complex singlet scalar extension of the 2HDM respecting a discrete dark *CP* symmetry, and simultaneously explain the observed DM relic density and the BAU via the spontaneous *CP* violation at high temperature. The dark *CP* symmetry allows the imaginary component of singlet scalar to have mixings with the pseudoscalars of scalar doublet fields, which play key roles in generating the *CP* violation sources needed by the EWBG at high temperature. On the other hand, the dark *CP* symmetry guarantees the real component to be a DM candidate.

*Corresponding author: leiwang@ytu.edu.cn

## II. 2HDM + S RESPECTING A DARK CP SYMMETRY

Imposing a discrete dark $CP$ symmetry, we extend the SM by a second Higgs doublet $\Phi_2$ and a complex singlet $S$,

$$\Phi_1 = \begin{pmatrix} \phi_1^+ \\ \frac{(v_1+\rho_1+i\eta_1)}{\sqrt{2}} \end{pmatrix}, \qquad \Phi_2 = \begin{pmatrix} \phi_2^+ \\ \frac{(v_2+\rho_2+i\eta_2)}{\sqrt{2}} \end{pmatrix}, \qquad S = \frac{(\chi + i\eta_s)}{\sqrt{2}}, \tag{2}$$

with $v_1$ and $v_2$ being the vacuum expectation values (VEVs), $v = \sqrt{v_1^2 + v_2^2} = (246\ \mathrm{GeV})^2$ and $\tan\beta \equiv v_2/v_1$. The singlet field $S$ has no VEV. Under the dark $CP$ symmetry, $S \to -S^*$ ($\chi \to -\chi, \eta_s \to \eta_s$ in the real parametrization), and while all the other fields are not affected.

The full scalar potential is given as

$$\begin{aligned} \mathrm{V} = {} & m_{11}^2(\Phi_1^\dagger\Phi_1) + m_{22}^2(\Phi_2^\dagger\Phi_2) + \frac{\lambda_1}{2}(\Phi_1^\dagger\Phi_1)^2 + \frac{\lambda_2}{2}(\Phi_2^\dagger\Phi_2)^2 + \lambda_3(\Phi_1^\dagger\Phi_1)(\Phi_2^\dagger\Phi_2) + \lambda_4(\Phi_1^\dagger\Phi_2)(\Phi_2^\dagger\Phi_1) \\ & + \left[\frac{\lambda_5}{2}(\Phi_1^\dagger\Phi_2)^2 + \lambda_6(\Phi_1^\dagger\Phi_1)(\Phi_1^\dagger\Phi_2) + \lambda_7(\Phi_2^\dagger\Phi_2)(\Phi_2^\dagger\Phi_1) + \mathrm{H.c.}\right] + m_S^2 SS^* + \left[\frac{m_S'^2}{2}SS + \mathrm{H.c.}\right] + \left[\frac{\lambda_1''}{24}S^4 + \mathrm{H.c.}\right] \\ & + \left[\frac{\lambda_2''}{6}S^2SS^* + \mathrm{H.c.}\right] + SS^*\left[\lambda_1'\Phi_1^\dagger\Phi_1 + \lambda_2'\Phi_2^\dagger\Phi_2\right] + \frac{\lambda_3''}{4}(SS^*)^2 + \left[S^2\left(\lambda_4'\Phi_1^\dagger\Phi_1 + \lambda_5'\Phi_2^\dagger\Phi_2\right) + \mathrm{H.c.}\right] \\ & + \left[\lambda_6'SS^*\Phi_2^\dagger\Phi_1 + \lambda_7'(SS + S^*S^*)\Phi_2^\dagger\Phi_1 + \mathrm{H.c.}\right] + \left[-m_{12}^2\Phi_2^\dagger\Phi_1 + \frac{\mu}{2}(S - S^*)\Phi_1^\dagger\Phi_2 + \mathrm{H.c.}\right], \end{aligned} \tag{3}$$

where all the coupling coefficients and mass are real, and thus the scalar potential sector is $CP$-conserved at zero temperature. The last term leads to the mixings of $\eta_s$ and the pseudoscalars of Higgs doublet fields, and $\chi$ is allowed to remain stable. For simplicity, we take $\lambda_6 = \lambda_7 = \lambda_6' = \lambda_7' = \lambda_2'' = 0$ in the following discussions.

The stationary conditions give

$$\begin{aligned} m_{11}^2 &= m_{12}^2 t_\beta - \frac{1}{2}v^2\left(\lambda_1 c_\beta^2 + \lambda_{345}s_\beta^2\right), \\ m_{22}^2 &= m_{12}^2/t_\beta - \frac{1}{2}v^2\left(\lambda_2 s_\beta^2 + \lambda_{345}c_\beta^2\right), \end{aligned} \tag{4}$$

where $t_\beta \equiv \tan\beta$, $s_\beta \equiv \sin\beta$, $c_\beta \equiv \cos\beta$, and $\lambda_{345} = \lambda_3 + \lambda_4 + \lambda_5$.

In addition to the 125 GeV Higgs $h$, the physical scalar spectrum contains a $CP$-even states $H$, a DM candidate $\chi$, two neutral pseudoscalars $A$ and $X$, and a charged scalar $H^\pm$. The mass eigenstates $h$, $H$, and $H^\pm$ and their masses are the same as those of the pure 2HDM. The $\eta_1$, $\eta_2$, and $\eta_s$ are rotated into the $A$, $X$, and $G$ by the two mixing angles $\theta$ and $\beta$, where $G$ is a Goldstone boson. The parameters $\mu$, $m_S^2$, and $m_S'^2$ are given as

$$\begin{aligned} m_S^2 &= \frac{1}{2}\left(m_\chi^2 + m_A^2 s_\theta^2 + m_X^2 c_\theta^2 - \lambda_1' v^2 c_\beta^2 - \lambda_2' v^2 s_\beta^2\right), \\ m_S'^2 &= \frac{1}{2}\left(m_\chi^2 - m_A^2 s_\theta^2 - m_X^2 c_\theta^2 - 2\lambda_4' v^2 c_\beta^2 - 2\lambda_5' v^2 s_\beta^2\right), \\ \mu &= \frac{\sqrt{2}\left(m_X^2 - m_A^2\right)}{v} s_\theta c_\theta, \end{aligned} \tag{5}$$

where $s_\theta \equiv \sin\theta$ and $c_\theta \equiv \cos\theta$. The couplings $\lambda_i$ ($i = 1, 2, 3, 4, 5$) are determined by

$$\begin{aligned} v^2\lambda_1 &= \frac{m_H^2 c_\alpha^2 + m_h^2 s_\alpha^2 - m_{12}^2 t_\beta}{c_\beta^2}, \qquad v^2\lambda_2 = \frac{m_H^2 s_\alpha^2 + m_h^2 c_\alpha^2 - m_{12}^2 t_\beta^{-1}}{s_\beta^2}, \\ v^2\lambda_3 &= \frac{(m_H^2 - m_h^2)s_\alpha c_\alpha + 2m_{H^\pm}^2 s_\beta c_\beta - m_{12}^2}{s_\beta c_\beta}, \qquad v^2\lambda_4 = \frac{(\hat{m}_A^2 - 2m_{H^\pm}^2)s_\beta c_\beta + m_{12}^2}{s_\beta c_\beta}, \\ v^2\lambda_5 &= \frac{-\hat{m}_A^2 s_\beta c_\beta + m_{12}^2}{s_\beta c_\beta}, \end{aligned} \tag{6}$$

with $\hat{m}_A^2 = m_A^2 c_\theta^2 + m_X^2 s_\theta^2$.

The general Yukawa interaction is given by

$$-\mathcal{L} = Y_{u2}\bar{Q}_L\tilde{\Phi}_2 u_R + Y_{d2}\bar{Q}_L\Phi_2 d_R + Y_{\ell 2}\bar{L}_L\Phi_2 e_R + Y_{u1}\bar{Q}_L\tilde{\Phi}_1 u_R + Y_{d1}\bar{Q}_L\Phi_1 d_R + Y_{\ell 1}\bar{L}_L\Phi_1 e_R + \text{H.c.}, \tag{7}$$

where $Q_L^T = (u_L, d_L)$, $L_L^T = (\nu_L, l_L)$, $\tilde{\Phi}_{1,2} = i\tau_2\Phi_{1,2}^*$, and $Y_{u1,2}$, $Y_{d1,2}$, and $Y_{\ell 1,2}$ are $3\times 3$ matrices in family space. The Yukawa coupling matrices are taken to be aligned to avoid the tree-level flavor changing neutral current [48,49],

$$\begin{aligned}
(Y_{u1})_{ii} &= \frac{\sqrt{2}m_{ui}}{v}\rho_{1u}, \qquad (Y_{u2})_{ii} = \frac{\sqrt{2}m_{ui}}{v}\rho_{2u},\\
(Y_{\ell 1})_{ii} &= \frac{\sqrt{2}m_{\ell i}}{v}\rho_{1\ell}, \qquad (Y_{\ell 2})_{ii} = \frac{\sqrt{2}m_{\ell i}}{v}\rho_{2\ell},\\
(X_{d1})_{ii} &= \frac{\sqrt{2}m_{di}}{v}\rho_{1d}, \qquad (X_{d2})_{ii} = \frac{\sqrt{2}m_{di}}{v}\rho_{2d},
\end{aligned} \tag{8}$$

where $X_{d1,2} = V_{\text{CKM}}^\dagger Y_{d1,2} V_{\text{CKM}}$, $\rho_{1f} = (c_\beta - s_\beta\kappa_f)$ and $\rho_{2f} = (s_\beta + c_\beta\kappa_f)$ with $f = u, d, \ell$. All the off-diagonal elements are zero. The couplings of the neutral Higgs bosons normalized to the SM are given by

$$\begin{aligned}
y_V^h &= \sin(\beta-\alpha), \qquad y_f^h = [\sin(\beta-\alpha) + \cos(\beta-\alpha)\kappa_f],\\
y_V^H &= \cos(\beta-\alpha), \qquad y_f^H = [\cos(\beta-\alpha) - \sin(\beta-\alpha)\kappa_f],\\
y_V^A &= 0, y_A^f = -i\kappa_f\,(\text{for } u)c_\theta, \qquad y_f^A = i\kappa_f c_\theta\,(\text{for } d,\ell),\\
y_V^X &= 0, y_X^f = -i\kappa_f\,(\text{for } u)s_\theta, \qquad y_f^X = i\kappa_f s_\theta\,(\text{for } d,\ell),
\end{aligned} \tag{9}$$

where $\alpha$ is the mixing angle of the two $CP$-even Higgs bosons, and $V$ denotes $Z$ or $W$. The Yukawa couplings of the charged Higgs are

$$\mathcal{L}_Y = -\frac{\sqrt{2}}{v}H^+\{\bar{u}_i[\kappa_d(V_{\text{CKM}})_{ij}m_{dj}P_R - \kappa_u m_{ui}(V_{\text{CKM}})_{ij}P_L]d_j + \kappa_\ell\bar{\nu}m_\ell P_R\ell\} + \text{H.c.}, \tag{10}$$

where $i, j = 1, 2, 3$ are the index of generation.

## III. RELEVANT THEORETICAL AND EXPERIMENTAL CONSTRAINTS

In our calculations, we consider the following theoretical and experimental constraints:

(1) The signal data of the 125 GeV Higgs. We take the light $CP$ even Higgs boson $h$ as the discovered 125 GeV state, and choose $\sin(\beta-\alpha) = 1$ to satisfy the bound of the 125 GeV Higgs signal data, for which the $h$ has the same tree-level couplings to the SM particles as the SM.

(2) The direct searches and indirect searches for extra Higgses. From the Eqs. (9) and (10), one see that the Yukawa couplings of the extra Higgses ($H$, $H^\pm$, $A$, $X$) are proportional to $\kappa_u$, $\kappa_d$ and $\kappa_\ell$ for $\sin(\beta-\alpha) = 1$. Therefore, $\kappa_u$, $\kappa_d$ and $\kappa_\ell$ can be small enough to suppress the production cross sections of these extra Higgses at the LHC, and satisfy the exclusion limits of searches for additional Higgs bosons at the LHC. Simultaneously, very small $\kappa_u$, $\kappa_d$ and $\kappa_\ell$ can accommodate the indirect searches for these extra Higgses via the $B$-meson decays. For example, for charged Higgs mass of 100 GeV, the measurements of $B_d \to \mu^+\mu^-$ and $B \to X_s\gamma$ exclude regions of $\kappa_u = \kappa_d = \kappa_\ell > \frac{1}{3}$ and $\kappa_u = \kappa_d = \kappa_\ell > \frac{1}{2}$, respectively [50]. In this paper we assume $\kappa_u \to 0$, $\kappa_d \to 0$, and $\kappa_\ell \to 0$, and ignore the effects of the three parameters in our following calculations and discussions while the constraints from the direct searches and indirect searches for extra Higgses are naturally satisfied.

(3) Vacuum stability. We require that the vacuum is stable at tree level, which means that the potential in Eq. (3) has to be bounded from below and the electroweak vacuum is the global minimum of the full scalar potential. To examine bounded from below condition we consider the minimum of quartic part in Eq. (3), $V_{4-\min}$, which is written in matrix form in the basis $B = (\Phi_1^\dagger\Phi_1,\ \Phi_2^\dagger\Phi_2,\ \chi^2,\ \eta_S^2)^T$,

$$V_{4-\min} = C^T\frac{1}{2}\underbrace{\begin{pmatrix} \lambda_1 & \lambda_3+\Delta & \lambda_1'+2\lambda_4' & \lambda_1'-2\lambda_4' \\ \lambda_3+\Delta & \lambda_2 & \lambda_2'+2\lambda_5' & \lambda_2'-2\lambda_5' \\ \lambda_1'+2\lambda_4' & \lambda_2'+2\lambda_5' & \frac{\lambda_1''+3\lambda_3''}{6} & \frac{-\lambda_1''+\lambda_3''}{2} \\ \lambda_1'-2\lambda_4' & \lambda_2'-2\lambda_5' & \frac{-\lambda_1''+\lambda_3''}{2} & \frac{\lambda_1''+3\lambda_3''}{6} \end{pmatrix}}_{A} C = \frac{1}{2}C^TAC, \tag{11}$$

where $\Delta = 0$ for $\lambda_4 \geq |\lambda_5|$ and $\Delta = \lambda_4 - |\lambda_5|$ for $\lambda_4 < |\lambda_5|$.

A copositive matrix $A$ is required to ensure the potential to be bounded from below. Following the approaches described in [51,52], the matrix $A$ need satisfy $\det(A) \geq 0 \vee (\mathrm{adj}A)_{ij} < 0$, for some $i$, $j$. The adjugate of $A$ is the transpose of the cofactor matrix of $A$: $(\mathrm{adj}A)_{ij} = (-1)^{i+j} M_{ji}$, with $M_{ij}$ being the determinant of the submatrix that results from deleting row $i$ and column $j$ of $A$. In addition, one deletes the $i$th row and column of $A$, $i = 1, 2, 3, 4$, and obtains 4 symmetric $3 \times 3$ matrices, which are required to be copositive. The copositivity of the symmetric order 3 matrix $B$ with entries $b_{ij}$, $i, j = 1, 2, 3$ requires

$$\begin{aligned}
&b_{11} \geq 0, \qquad b_{22} \geq 0, \qquad b_{33} \geq 0,\\
&\bar{b}_{12} = b_{12} + \sqrt{b_{11} b_{22}} \geq 0,\\
&\bar{b}_{13} = b_{13} + \sqrt{b_{11} b_{33}} \geq 0,\\
&\bar{b}_{23} = b_{23} + \sqrt{b_{22} b_{33}} \geq 0,\\
&\sqrt{b_{11} b_{22} b_{33}} + b_{12}\sqrt{b_{33}} + b_{13}\sqrt{b_{22}} + b_{23}\sqrt{b_{11}} + \sqrt{2\bar{b}_{12}\bar{b}_{13}\bar{b}_{23}} \geq 0.
\end{aligned} \tag{12}$$

(4) Tree-level perturbative unitarity. We demand that the amplitudes of the scalar quartic interactions leading to $2 \to 2$ scattering processes remain below the value of $8\pi$ at tree-level, which is implemented in SPheno-v4.0.5 [53] using SARAH-SPheno files [54].

(5) The oblique parameters. The oblique parameters ($S$, $T$, $U$) can obtain additional corrections via the self-energy diagrams exchanging $H$, $H^{\pm}$, $A$, and $X$. For $\sin(\beta - \alpha) = 1$, the expressions of $S$, $T$ and $U$ in the model are approximately written as [55,56]

$$\begin{aligned}
S &= \frac{1}{\pi m_Z^2}\left[c_\theta^2 F_S\left(m_Z^2, m_H^2, m_A^2\right) + s_\theta^2 F_S\left(m_Z^2, m_H^2, m_X^2\right) - F_S\left(m_Z^2, m_{H^\pm}^2, m_{H^\pm}^2\right)\right],\\
T &= \frac{1}{16\pi m_W^2 s_W^2}\left[-c_\theta^2 F_T\left(m_H^2, m_A^2\right) - s_\theta^2 F_T\left(m_H^2, m_X^2\right) + F_T\left(m_{H^\pm}^2, m_H^2\right) + c_\theta^2 F_T\left(m_{H^\pm}^2, m_A^2\right) + s_\theta^2 F_T\left(m_{H^\pm}^2, m_X^2\right)\right],\\
U &= \frac{1}{\pi m_W^2}\left[F_S(m_W^2, m_{H^\pm}^2, m_H^2) - 2F_S\left(m_W^2, m_{H^\pm}^2, m_{H^\pm}^2\right) + c_\theta^2 F_S\left(m_W^2, m_{H^\pm}^2, m_A^2\right) + s_\theta^2 F_S\left(m_W^2, m_{H^\pm}^2, m_X^2\right)\right]\\
&\quad - \frac{1}{\pi m_Z^2}\left[c_\theta^2 F_S\left(m_Z^2, m_H^2, m_A^2\right) + s_\theta^2 F_S\left(m_Z^2, m_H^2, m_X^2\right) - F_S\left(m_Z^2, m_{H^\pm}^2, m_{H^\pm}^2\right)\right],
\end{aligned} \tag{13}$$

where

$$F_T(a,b) = \frac{1}{2}(a+b) - \frac{ab}{a-b}\log\left(\frac{a}{b}\right), \qquad F_S(a,b,c) = B_{22}(a,b,c) - B_{22}(0,b,c), \tag{14}$$

with

$$\begin{aligned}
B_{22}(a,b,c) &= \frac{1}{4}\left[b + c - \frac{1}{3}a\right] - \frac{1}{2}\int_0^1 dx\, X \log(X - i\epsilon),\\
X &= bx + c(1-x) - ax(1-x).
\end{aligned} \tag{15}$$

Reference [1] gave the fit results of $S$, $T$, and $U$,

$$S = -0.01 \pm 0.10, \qquad T = 0.03 \pm 0.12, \qquad U = 0.02 \pm 0.11, \tag{16}$$

with the correlation coefficients

$$\rho_{ST} = 0.92, \qquad \rho_{SU} = -0.80, \qquad \rho_{TU} = -0.93. \tag{17}$$

## IV. DARK MATTER

The two neutral $CP$-even Higgs can mediate the interactions of DM, $\lambda_h v\chi^2 h/2$ and $\lambda_H v\chi^2 H/2$ with

$$\lambda_h \equiv (\lambda_2' + 2\lambda_5')vs_\beta c_\alpha - (\lambda_1' + 2\lambda_4')vc_\beta s_\alpha,$$
$$\lambda_H \equiv (\lambda_2' + 2\lambda_5')vs_\beta s_\alpha + (\lambda_1' + 2\lambda_4')vc_\beta c_\alpha. \quad (18)$$

We consider a light DM whose freeze-out temperature is much lower than that of EWPT, and thus the effect of EWPT on the current DM relic density can be ignored. We take the new scalars to be much heavier than the DM so that the DM pair-annihilation to these new scalars are kinematically forbidden. In the parameter space chosen previously, the couplings of $H$ to the SM particles can be ignored. Therefore, the DM relic density hardly constrains the $\lambda_H$, and $\lambda'_{1,2,4,5}$ are allowed to have room enough to produce the pattern of EWPT needed by the EWBG. The annihilation processes with $s$-channel exchange of $h$ are responsible for the relic density. However, for a light $\chi$, the invisible decay $h \to \chi\chi$ is kinematically allowed, and the signal data of the 125 GeV Higgs impose strong upper limits on the $h\chi\chi$ coupling [57], which is possible to conflict with the requirement of the correct relic density The elastic scattering of $\chi$ on a nucleon receives the contributions of the process with $t$-channel exchange of $h$, which can be strongly constrained by the direct searches experiments of XENON [58]. Besides, the indirect searches for DM can impose upper limits on the averaged cross sections of the DM annihilation to $e^+e^-$, $\mu^+\mu^-$, $\tau^+\tau^-$, $u\bar{u}$, $b\bar{b}$, and $WW$ [59].

After imposing the relevant theoretical and experimental constraints mentioned previously, we show the $\lambda_h$ versus $m_\chi$ allowed by the invisible decay of the 125 GeV Higgs, the DM relic density, the direct and indirect searches experiments in Fig. 1. From Fig. 1, we find that the DM with a mass of 55 GeV–62.5 GeV is allowed by the joint constraints of the invisible decay of the 125 GeV Higgs, the DM relic density, the direct and indirect searches experiments.

## V. EWPT AND BARYOGENESIS

We first consider the effective scalar potential at the finite temperature. The neutral elements of $\Phi_1$ and $\Phi_2$ are shifted by $\frac{h_1}{\sqrt{2}}$ and $\frac{h_2+ih_3}{\sqrt{2}}$. It is plausible to take the imaginary part of the neutral elements of $\Phi_1$ to be zero since the effective potential of Eq. (3) only depends on the relative phase of the neutral elements of $\Phi_1$ and $\Phi_2$.

The complete effective potential at finite temperature contains the tree level potential, the Coleman-Weinberg term [60], the finite temperature corrections [61] and the resummed daisy corrections [62,63], which is gauge-dependent [64,65]. Here we consider the high-temperature approximation of effective potential, which keeps only the thermal mass terms in the high-temperature expansion and the tree-level potential. Therefore, the effective potential is gauge invariant, and it does not depend on the renormalization scheme and the resummation scheme. The high-temperature approximation of effective potential is given by

$$\begin{aligned}
V_{\rm eff}(h_1,h_2,h_3,\chi,\eta_s) &= \frac{1}{2}(m_{11}^2+\Pi_{h_1})h_1^2 + \frac{1}{2}(m_{22}^2+\Pi_{h_2})(h_2^2+h_3^2) + \frac{1}{2}(m_S^2+m_S'^2+\Pi_\chi)\chi^2 + \frac{1}{2}(m_S^2-m_S'^2+\Pi_{\eta_s})\eta_s^2 \\
&+ \frac{1}{8}(\lambda_1 h_1^4+\lambda_2 h_2^4+\lambda_2 h_3^4) + \frac{1}{4}\lambda_{345}h_1^2h_2^2 + \frac{1}{4}\bar{\lambda}_{345}h_1^2h_3^2 + \frac{\lambda_2}{4}h_3^2h_2^2 - m_{12}^2h_1h_2 - \frac{\mu}{\sqrt{2}}h_3\eta_s h_1 \\
&+ \frac{\lambda_1'}{4}(\chi^2+\eta_s^2)h_1^2 + \frac{\lambda_2'}{4}(\chi^2+\eta_s^2)(h_2^2+h_3^2) + \frac{\lambda_4'}{2}(\chi^2-\eta_s^2)h_1^2 + \frac{\lambda_5'}{2}(\chi^2-\eta_s^2)(h_3^2+h_2^2) \\
&+ \left(\frac{\lambda_1''}{48}+\frac{\lambda_3''}{16}\right)(\chi^4+\eta_s^4) + \frac{1}{8}(\lambda_3''-\lambda_1'')\chi^2\eta_s^2, \\
\Pi_{h_1} &= \left[\frac{9g^2}{2}+\frac{3g'^2}{2}+6\lambda_1+4\lambda_3+2\lambda_4+2\lambda_1'+6y_t^2c_\beta^2\right]\frac{T^2}{24}, \\
\Pi_{h_2} &= \left[\frac{9g^2}{2}+\frac{3g'^2}{2}+6\lambda_2+4\lambda_3+2\lambda_4+2\lambda_2'+6y_t^2s_\beta^2\right]\frac{T^2}{24}, \\
\Pi_{h_3} &= \Pi_{h_2}, \\
\Pi_\chi &= [4\lambda_1'+4\lambda_2'+8\lambda_4'+8\lambda_5'+2\lambda_3'']\frac{T^2}{24}, \\
\Pi_{\eta_s} &= [4\lambda_1'+4\lambda_2'-8\lambda_4'-8\lambda_5'+2\lambda_3'']\frac{T^2}{24}, \quad (19)
\end{aligned}$$

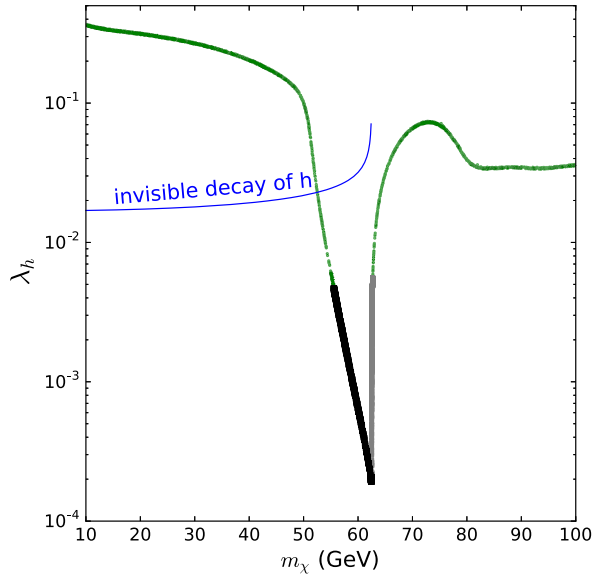


FIG. 1. $\lambda_h$ consistent with the relic data versus $m_\chi$. The dark thick line is allowed by the direct and indirect searches for DM, and the light thick line is excluded by the indirect searches.

where $\bar{\lambda}_{345} = \lambda_3 + \lambda_4 - \lambda_5$, $y_t = \frac{\sqrt{2}m_t}{v}$, and $\Pi_i$ denotes the thermal mass terms of the field $i$.

Because baryogenesis is driven by diffusion processes in front of the bubble wall, one needs to compute the $T_n$ at which bubble nucleation actually starts. This can be calculated straightforwardly from the nucleation rate per unit volume by [66–68], $\Gamma \approx A(T)e^{-S_3/T}$, where $A(T) \sim T^4$ is a prefactor and $S_3$ is a three-dimensional Euclidian action. The nucleation temperature $T_n$ is obtained by $\Gamma/H^4 = 1$, where $H$ is the Hubble parameter. It is roughly estimated by $\frac{S_3(T)}{T}|_{T=T_n} = 140$. The bubble wall VEV profiles can be determined by the bounce equations of fields.

The WKB approximation method is used to evaluate the $CP$-violating source terms and chemical potentials transport equations of particle species in the wall frame with a radial coordinate $z$ [22,69,70]. A top quark penetrating the bubble wall acquires a complex mass as a function of $z$,

$$m_t(z) = \frac{y_t}{\sqrt{2}}\sqrt{(c_\beta h_1(z) + s_\beta h_2(z))^2 + s_\beta^2 h_3^2(z)}\, e^{i\Theta_t(z)},$$

$$\text{with} \quad \Theta_t(z) = \varphi_Z(z) + \arctan\frac{s_\beta h_3(z)}{c_\beta h_1(z) + s_\beta h_2(z)},$$

$$\partial_z\varphi_Z(z) = -\frac{h_2^2(z) + h_3^2(z)}{h_1^2(z) + h_2^2(z) + h_3^2(z)}\partial_z\varphi(z),$$

$$\varphi(z) = \arctan\frac{h_3(z)}{h_2(z)}. \tag{20}$$

In our calculation, the imaginary part of the neutral element of $\Phi_1$ is taken to be zero. As a result, the nonvanishing $Z_\mu$ field induces an additional $CP$-violating force acting on the top quark, which is removed a local axial transformation of top quark, reintroducing an additional overall phase $\varphi_Z(z)$ into $m_t$ [27].

The transport equations are derived by the complex mass of the top quark, and contains effects of the strong sphaleron process ($\Gamma_{ss}$) [22,71], W-scattering ($\Gamma_W$) [22,72], the top Yukawa interaction ($\Gamma_y$) [22,72], the top helicity flips ($\Gamma_M$) [22,72], and the Higgs number violation ($\Gamma_h$) [22,72]. The transport equations are written as

$$\begin{aligned}
0 &= 3v_W K_{1,t}(\partial_z\mu_{t,2}) + 3v_W K_{2,t}(\partial_z m_t^2)\mu_{t,2} + 3(\partial_z u_{t,2}) - 3\Gamma_y(\mu_{t,2} + \mu_{t^c,2} + \mu_{h,2}) - 6\Gamma_M(\mu_{t,2} + \mu_{t^c,2}) - 3\Gamma_W(\mu_{t,2} - \mu_{b,2}) \\
&\quad - 3\Gamma_{ss}[(1 + 9K_{1,t})\mu_{t,2} + (1 + 9K_{1,b})\mu_{b,2} + (1 - 9K_{1,t})\mu_{t^c,2}], \\
0 &= 3v_W K_{1,t}(\partial_z\mu_{t^c,2}) + 3v_W K_{2,t}(\partial_z m_t^2)\mu_{t^c,2} + 3(\partial_z u_{t^c,2}) - 3\Gamma_y(\mu_{t,2} + \mu_{b,2} + 2\mu_{t^c,2} + 2\mu_{h,2}) - 6\Gamma_M(\mu_{t,2} + \mu_{t^c,2}) \\
&\quad - 3\Gamma_{ss}[(1 + 9K_{1,t})\mu_{t,2} + (1 + 9K_{1,b})\mu_{b,2} + (1 - 9K_{1,t})\mu_{t^c,2}], \\
0 &= 3v_W K_{1,b}(\partial_z\mu_{b,2}) + 3(\partial_z u_{b,2}) - 3\Gamma_y(\mu_{b,2} + \mu_{t^c,2} + \mu_{h,2}) - 3\Gamma_W(\mu_{b,2} - \mu_{t,2}), \\
&\quad - 3\Gamma_{ss}[(1 + 9K_{1,t})\mu_{t,2} + (1 + 9K_{1,b})\mu_{b,2} + (1 - 9K_{1,t})\mu_{t^c,2}], \\
0 &= 4v_W K_{1,h}(\partial_z\mu_{h,2}) + 4(\partial_z u_{h,2}) - 3\Gamma_y(\mu_{t,2} + \mu_{b,2} + 2\mu_{t^c,2} + 2\mu_{h,2}) - 4\Gamma_h\mu_{h,2}, \\
S_t &= -3K_{4,t}(\partial_z\mu_{t,2}) + 3v_W\tilde{K}_{5,t}(\partial_z u_{t,2}) + 3v_W\tilde{K}_{6,t}(\partial_z m_t^2)u_{t,2} + 3\Gamma_t^{\text{tot}}u_{t,2}, \\
0 &= -3K_{4,b}(\partial_z\mu_{b,2}) + 3v_W\tilde{K}_{5,b}(\partial_z u_{b,2}) + 3\Gamma_b^{\text{tot}}u_{b,2}, \\
S_t &= -3K_{4,t}(\partial_z\mu_{t^c,2}) + 3v_W\tilde{K}_{5,t}(\partial_z u_{t^c,2}) + 3v_W\tilde{K}_{6,t}(\partial_z m_t^2)u_{t^c,2} + 3\Gamma_t^{\text{tot}}u_{t^c,2}, \\
0 &= -4K_{4,h}(\partial_z\mu_{h,2}) + 4v_W\tilde{K}_{5,h}(\partial_z u_{h,2}) + 4\Gamma_h^{\text{tot}}u_{h,2},
\end{aligned} \tag{21}$$

The $\mu_{i,2}$ and $u_{i,2}$ are the second-order $CP$-odd chemical potential and the plasma velocity of the particle $i = t, t^c, b, h,$. The source term $S_t$ is

$$S_t = -v_W K_{8,t}\partial_z(m_t^2\partial_z\theta_t) + v_W K_{9,t}(\partial_z\theta_t)m_t^2(\partial_z m_t^2). \quad (22)$$

The functions $K_{a,i}$ and $\tilde{K}_{a,i}$ $(a = 1\text{–}9)$ are defined in Ref. [70], and the $\Gamma_i^{\rm tot}$ are the total reaction rate of the particle $i$ [22,70].

The chemical potential of the left-handed quarks $\mu_{B_L}$ is obtained by solving the transport equations. The left-handed quark number is converted into a baryon asymmetry by the weak sphalerons, which is calculated as

$$Y_B = \frac{405\Gamma_{ws}}{4\pi^2 v_w g_* T_n}\int_0^\infty dz\mu_{B_L}(z)f_{\rm sph}(z)\exp\left(-\frac{45\Gamma_{ws}z}{4v_w}\right), \quad (23)$$

where $\Gamma_{ws} \simeq 10^{-6}T_n$ is the weak sphaleron rate inside bubble [73] and the wall velocity $v_w$ is taken as 0.1. The function $f_{\rm sph}(z) = \min(1, 2.4\frac{T_n}{\Gamma_{ws}}e^{-40\xi_n(z)/T_n})$ with $\xi_n(z) = \sqrt{\langle h_1\rangle^2 + \langle h_2\rangle^2 + \langle h_3\rangle^2}$ is used to smoothly interpolate between the sphaleron rates in the broken and unbroken phases [27].

Now we discuss the pattern of PTs which can achieve the spontaneous $CP$ violation at a finite temperature and recover the $CP$ symmetry at the present temperature. The $CP$ symmetry is conserved both at a very high temperature and the present temperature. Therefore, the $CP$ violation does not appear if the Universe only undergoes a single-step PT. Next, we assume that the Universe undergoes a two-step PTs, and the first-step PT is a strongly first-order PT converting the origin phase of $h_{1,2,3}$ and $\eta_s$ into a broken phase simultaneously. Thus, the $CP$ symmetry is spontaneously broken, and then BAU can be generated during the process of the first-step PT. After the second-step PT, the observed vacuum is produced and the $CP$ symmetry is restored. However, the effective potential $V_{\rm eff}$ in Eq. (19) presents an unbroken $Z_2$ symmetry under which $h_3 \to -h_3$ and $\eta_s \to -\eta_s$. As a result, there will not be a bias between transitions to $(\langle h_1\rangle, \langle h_2\rangle, \langle h_3\rangle, \langle\chi\rangle, \langle\eta_s\rangle)$ and $(\langle h_1\rangle, \langle h_2\rangle, -\langle h_3\rangle, \langle\chi\rangle, -\langle\eta_s\rangle)$ from the origin (0, 0, 0, 0, 0) GeV. Therefore, there are two kinds of bubbles relating to $\Theta_t$ and $-\Theta_t$, and they produce baryon asymmetry of opposite signs. Eventually, the averaged baryon number in whole region is zero because of their opposite signs. As discussed in Ref. [47], in order to solve the problem, one may try to introduce a $Z_2$ symmetry breaking term, $-i\mu_3(S - S^*)^3$, which leads to a potential difference between the vacua with $\pm\langle\eta_s\rangle$, $\Delta V$. If $\Delta V$ is large enough so that the volumes occupied by the $\pm\langle\eta_s\rangle$ phases can be significantly different, the net baryon number in whole region will be nonzero [74,75]. Unfortunately, to explain the observed BAU, $\mu_3$ need have a non-negligible value compared to other parameters of potential, which is incompatible with the expected spontaneous $CP$ violation at a finite temperature since the $\mu_3$ term breaks the $CP$ symmetry explicitly. The problem can be well solved via a three-step PTs. At the first-step PT, the $\eta_S$ field firstly acquires a nonzero VEV while $\langle h_{1,2,3}\rangle$ and $\langle\chi\rangle$ still remain zero. The second-step PT is a strongly first-order EWPT converting the origin phase of $h_{1,2,3}$ into an electroweak symmetry broken phase, where $h_3$ is required to be nonzero. In order to prevent the electroweak sphalerons to wash out the produced BAU inside the bubbles of broken phase, the PT strength is impose an bound [76], $\frac{\xi_n}{T_n} > 1.0$ in the broken phase. After the third-step PT, the observed vacuum is produced and the $CP$ symmetry is restored while the BAU is not changed. The first-step PT is the $Z_2$-breaking PT, which means that two different domains with $\pm\langle\eta_s\rangle$ can appear. The temperature at the first-step PT can be significantly higher than the temperature of the EWPT at the second-step PT. The regions with $-\langle\eta_s\rangle$ can vanish when the EWPT takes place. The needed condition is $\Delta V/T^4 > 10^{-16}$ [77,78], which can be satisfied by $\mu_3$ around $\mathcal{O}(10^{-14})$ GeV. For such small $\mu_3$ term, the $CP$-conservation is a safe approximation in the model.

We employ the package CosmoTransitions to analyze the PTs [79]. Some parameter space achieving the three-step PTs are shown in Fig. 2, where we consider the constraints of the vacuum stability, oblique parameter [1], dark matter observables, and the 125 GeV Higgs signal data, and the data of BAU is not included. From Fig. 2, we find that the three-step PTs satisfying our requirements favor an appropriate value of $\mu$ since the $\mu$ term of Eq. (19) can lead to a close correlation between $\langle h_3\rangle$ and $\langle\eta_s\rangle$ of the potential minimum. As a result, according to Eq. (5), $m_A$ and $m_X$ is required to have a large mass splitting.

We pick out a benchmark point BP1 to discuss the EWPT and baryogenesis in detail, and the key input

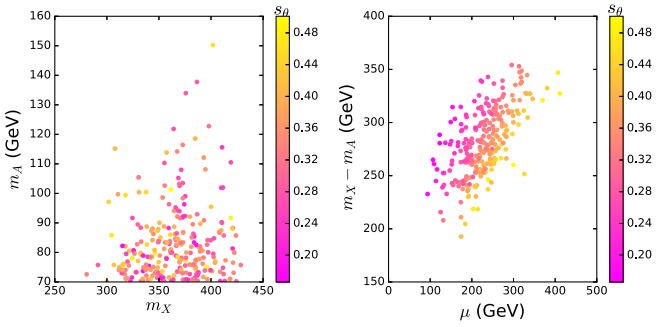


FIG. 2. The scattering plots achieving the three-step PTs with the characteristics mentioned in the text, where we take $m_H = m_{H^\pm}$ and $0.1 < s_\theta < 0.7$.

TABLE I. Input parameters for the BP1, and other parameters are given above.

| $m_h$ (GeV) | $m_H = m_{H^\pm}$ (GeV) | $m_\chi$ (GeV) | $m_A$ (GeV) | $m_X$ (GeV) | $m_{12}^2$ $(\text{GeV})^2$ |
|---|---|---|---|---|---|
| 125.0 | 467.69 | 55.95 | 69.80 | 333.67 | 2740.09 |

| $t_\beta$ | $\sin(\beta-\alpha)$ | $\sin\theta$ | $\lambda_1'$ | $\lambda_2'$ | $\lambda_4'$ | $\lambda_5'$ | $\lambda_1'' = \lambda_3''$ |
|---|---|---|---|---|---|---|---|
| 1.0 | 1.0 | 0.324 | 2.293 | 1.351 | −1.143 | −0.675 | 1.839 |

parameters are shown in Table I. The phase histories for the BP1 are shown in Fig. 3. Because the contributions of the thermal mass terms to the effective potential are proportional to $T^2$, the minimum of the potential is at the origin at a very high temperature. As the Universe cools, at T = 85.38 GeV, a second-order PT takes place during which $\eta_s$ acquires a nonzero VEV and the other four fields remain zero. At T = 69.65 GeV, a strongly first-order EWPT starts which breaks electroweak symmetry, $(0, 0, 0, 0, 73.71)$ GeV $\rightarrow$ $(62.42, 34.64, 55.24, 0.0, 37.50)$ GeV for $(\langle h_1\rangle, \langle h_2\rangle, \langle h_3\rangle, \langle\chi\rangle, \langle\eta_s\rangle)$. The PT strength is 1.30, and the BAU is produced via the EWBG mechanism. At T = 52.95 GeV, another second-order PT happens, and then $CP$ symmetry is recovered. The vacuum evolves along the final phase, and ultimately ends in the observed values at T = 0 GeV. Meanwhile, $\xi_n > 1$ is always kept so that the BAU is not washed out by the sphaleron processes. The freeze-out temperature of $\chi$ with a mass of 55.95 GeV is around 2.8 GeV, which is much lower than the PT temperatures.

The calculation of BAU depends on the bubble wall profiles, and we use the FindBounce [80] to obtain the bubble wall VEV profiles for the first-order EWPT of BP1, which is given in Fig. 4. The WKB method of calculating transport equations needs the condition of $L_W T_n \gg 1$, where $L_W$ is the width of bubble wall. The $L_W T_n$ of BP1 is approximately estimated to be 3.4.

We solve the transport equations with the boundary conditions $\mu_i\,(z = \pm\infty) = 0\,(i = t, t^c, b, h)$, and obtain the chemical potentials $\mu_i$ and velocity perturbations $u_i$ of each particle species. We show the $\mu_i$ and $u_i$ for the BP1 in

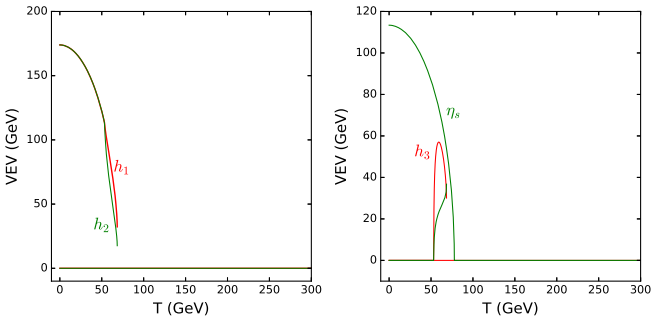


FIG. 3. The phase histories of the BP1, where $\langle\chi\rangle$ is always 0.

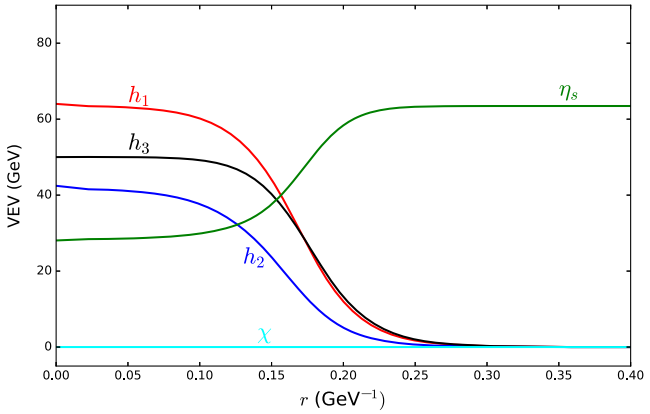


FIG. 4. The radial nucleation bubble wall VEV profiles for the first-order EWPT.

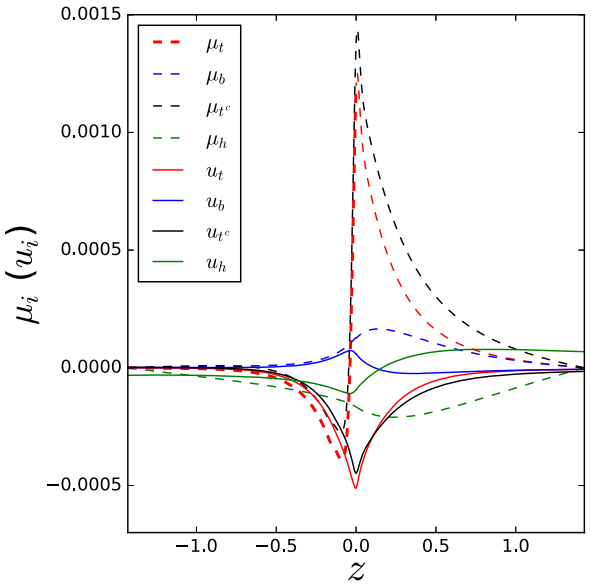


FIG. 5. The $\mu_i$ and $u_i$ from the transport equations as functions of the position of the bubble wall.

Fig. 5, which give rise to the BAU, $Y_B \simeq 8.4 \times 10^{-11}$. Figure 6 displays $Y_B$ as a function of the wall velocity $v_w$ for the BP1. $Y_B$ tends to decrease with an increase of $v_w$, and it does change strongly in the range of $v_w < 0.4$.

In Fig. 7, we show the dependences of $Y_B$ on $\tan\beta$ and $\mu$. The $\tan\beta$ denotes the ratio of $\langle h_1\rangle$ and $\langle h_2\rangle$ at zero temperature, and the $\mu$ term of Eq. (19) leads to a close correlation between $\langle h_3\rangle$ and $\langle\eta_s\rangle$ of the potential minimum at a finite temperature, which can play key roles in the $CP$-violating source term. We find that $Y_B$ can have a large value for moderate values of $\tan\beta$ and $\mu$, $\tan\beta$ around 1.2 and $\mu$ around 2500 GeV. We roughly estimate that the $-i\mu_3(S - S^*)^3$ term with $\mu_3$ being $\mathcal{O}(10^{-15})$ GeV can eliminate the region with $\langle\eta_s\rangle$ of opposite sign when the EWPT takes place, and the result of BAU is not affected.

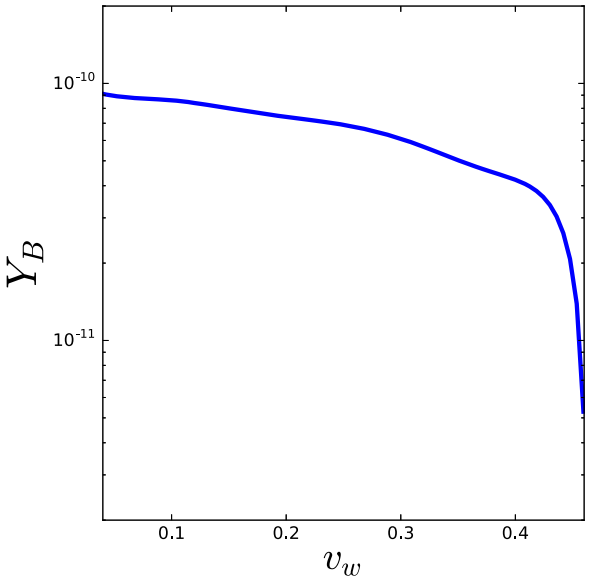


FIG. 6. $Y_B$ as a function of $v_w$ for the BP1.

## VI. COMMENT ON GRAVITATIONAL WAVE SIGNATURES, DARK MATTER, AND THE LHC SIGNATURES

The first-order EWPT needed by the EWBG can produce the gravitational wave. We find that the gravitational wave signatures from the three-step PTs mentioned above can easily exceed the sensitivity curve of the U-DECIGO detector [81], such as those of BP1. A full exploration of the parameter space will potentially find promising regions for detectable gravitational wave signal at the BBO [82]. The extra Higgses ($H$, $H^{\pm}$, $A$, $X$) couplings to the SM fermions are significantly suppressed for $\kappa_{u,d,\ell} \to 0$. Therefore, these extra Higgses are dominantly produced at the LHC via the electroweak processes mediated by $Z$, $W^{\pm}$, and $\gamma$, and the main decay modes include $H \to AZ$, $H^{\pm} \to AW^{\pm}$. The $A$ decay modes depend on specific values of $\kappa_{u,d,\ell}$. For a heavy DM whose freeze-out temperature is higher than the EWPT temperature, the EWPT can give significant effects on the DM relic density. The studies of the LHC signatures and the heavy DM will be carried out in the future.

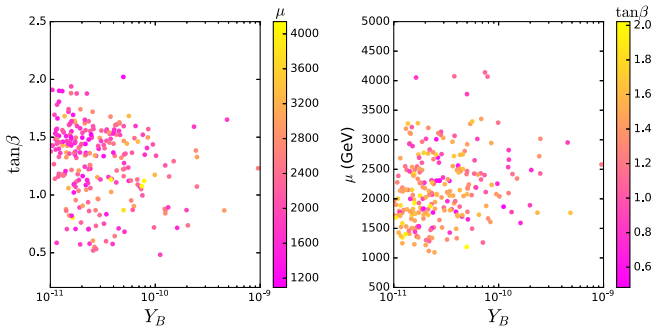


FIG. 7. $Y_B$ versus $\tan\beta$ and $Y_B$ versus $\mu$ for the left panel and right panel.

## VII. CONCLUSION

We proposed a complex singlet scalar extension of the 2HDM respecting a discrete dark $CP$ symmetry. The dark $CP$ symmetry guarantees $\chi$ to be a DM candidate on one hand and on the other hand allows $\eta_s$ to have mixings with the pseudoscalars of the scalar doublet fields, which plays key roles in producing the $CP$ violation sources needed by the EWBG at high temperature. Imposing relevant theoretical and experimental constraints, we studied the scenario of $m_\chi$ around the SM Higgs resonance region, and found that the dark matter relic abundance and the BAU can be simultaneously explained.

## ACKNOWLEDGMENTS

This work was supported by the Natural Science Foundation of Shandong Province ZR2023MA038, and the National Natural Science Foundation of China under Grant No. 11975013.

[1] P. A. Zyla *et al.* (Particle Data Group), Review of particle physics, Prog. Theor. Exp. Phys. **2020**, 083C01 (2020).
[2] A. D. Sakharov, Violation of $CP$ invariance, C asymmetry, and baryon asymmetry of the universe, Pisma Zh. Eksp. Teor. Fiz. **5**, 32 (1967).
[3] V. A. Kuzmin, V. A. Rubakov, and M. E. Shaposhnikov, On anomalous electroweak baryon-number non-conservation in the early universe, Phys. Lett. **155B**, 36 (1985).
[4] V. A. Rubakov and M. E. Shaposhnikov, Electroweak baryon number non-conservation in the early Universe and in high-energy collisions, Usp. Fiz. Nauk **166**, 493 (1996) [Phys. Usp. **39**, 461 (1996)].
[5] J. McDonald, Electroweak baryogenesis and dark matter via a gauge singlet scalar, Phys. Lett. B **323**, 339 (1994).
[6] G. C. Branco, D. Delepine, D. Emmanuel-Costa, and F. R. Gonzalez, Electroweak baryogenesis in the presence of an isosinglet quark, Phys. Lett. B **442**, 229 (1998).
[7] V. Barger, P. Langacker, M. McCaskey, M. Ramsey-Musolf, and G. Shaughnessy, Complex singlet extension of the standard model, Phys. Rev. D **79**, 015018 (2009).

[8] S. Profumo, M. J. Ramsey-Musolf, and G. Shaughnessy, Singlet Higgs phenomenology and the electroweak phase transition, J. High Energy Phys. 08 (2007) 010.

[9] F. P. Huang, Z. Qian, and M. Zhang, Exploring dynamical *CP* violation induced baryogenesis by gravitational waves and colliders, Phys. Rev. D **98**, 015014 (2018).

[10] A. Beniwal, M. Lewicki, M. White, and A. G. Williams, Gravitational waves and electroweak baryogenesis in a global study of the extended scalar singlet model, J. High Energy Phys. 02 (2019) 183.

[11] M. Jiang, L. Bian, W. Huang, and J. Shu, Impact of a complex singlet: Electroweak baryogenesis and dark matter, Phys. Rev. D **93**, 065032 (2016).

[12] P. H. Ghorbani, Electroweak baryogenesis and dark matter via a pseudoscalar vs. scalar, J. High Energy Phys. 08 (2017) 058.

[13] W. Chao, *CP* violation at the finite temperature, Phys. Lett. B **796**, 102 (2019).

[14] B. Grzadkowski and D. Huang, Spontaneous *CP*-violating electroweak baryogenesis and dark matter from a complex singlet scalar, J. High Energy Phys. 08 (2018) 135.

[15] K. P. Xie, Lepton-mediated electroweak baryogenesis, gravitational waves and the $4\tau$ final state at the collider, J. High Energy Phys. 02 (2021) 090; 08 (2022) 052(E).

[16] M. Lewicki, M. Merchand, and M. Zych, Electroweak bubble wall expansion: Gravitational waves and baryogenesis in standard model-like thermal plasma, J. High Energy Phys. 02 (2022) 017.

[17] J. Ellis, M. Lewicki, M. Merchand, J. M. No, and M. Zych, The scalar singlet extension of the standard model: Gravitational waves versus baryogenesis, J. High Energy Phys. 01 (2023) 093.

[18] C. Idegawa and E. Senaha, Electron electric dipole moment and electroweak baryogenesis in a complex singlet extension of the Standard Model with degenerate scalars, Phys. Lett. B **848**, 138332 (2024).

[19] K. Harigaya and I. R. Wang, First-order electroweak phase transition and baryogenesis from a naturally light singlet scalar, arXiv:2207.02867.

[20] N. Turok and J. Zadrozny, Electroweak baryogenesis in the two doublet model, Nucl. Phys. **B358**, 471 (1991).

[21] J. M. Cline, K. Kainulainen, and A. P. Vischer, Dynamics of two-Higgs-doublet CP violation and baryogenesis at the electroweak phase transition, Phys. Rev. D **54**, 2451 (1996).

[22] L. Fromme, S. J. Huber, and M. Seniuch, Baryogenesis in the two-Higgs doublet model, J. High Energy Phys. 11 (2006) 038.

[23] S. Kanemura, Y. Okada, and E. Senaha, Electroweak baryogenesis and quantum corrections to the triple Higgs boson coupling, Phys. Lett. B **606**, 361 (2005).

[24] P. Basler, M. Mühlleitner, and J. Wittbrodt, The *CP*-violating 2HDM in light of a strong first order electroweak phase transition and implications for Higgs pair production, J. High Energy Phys. 03 (2018) 061.

[25] T. Abe, J. Hisano, T. Kitahara, and K. Tobioka, Gauge invariant Barr-Zee type contributions to fermionic EDMs in the two-Higgs doublet models, J. High Energy Phys. 01 (2014) 106; 04 (2016) 161(E).

[26] S. Tulin and P. Winslow, Anomalous B meson mixing and baryogenesis, Phys. Rev. D **84**, 034013 (2011).

[27] J. M. Cline, K. Kainulainen, and M. Trott, Electroweak baryogenesis in two Higgs doublet models and B meson anomalies, J. High Energy Phys. 11 (2011) 089.

[28] T. Liu, M. J. Ramsey-Musolf, and J. Shu, Electroweak beautygenesis: From $b \to s$ *CP* violation to the cosmic baryon asymmetry, Phys. Rev. Lett. **108**, 221301 (2012).

[29] M. Ahmadvand, Baryogenesis within the two-Higgs-doublet model in the electroweak scale, Int. J. Mod. Phys. A **29**, 1450090 (2014).

[30] C. W. Chiang, K. Fuyuto, and E. Senaha, Electroweak baryogenesis with lepton flavor violation, Phys. Lett. B **762**, 315 (2016).

[31] H. K. Guo, Y. Y. Li, T. Liu, M. Ramsey-Musolf, and J. Shu, Lepton-flavored electroweak baryogenesis, Phys. Rev. D **96**, 115034 (2017).

[32] T. Modak and E. Senaha, Electroweak baryogenesis via bottom transport, Phys. Rev. D **99**, 115022 (2019).

[33] P. Basler, M. Mühlleitner, and J. Müller, BSMPT v2 a tool for the electroweak phase transition and the baryon asymmetry of the universe in extended Higgs sectors, Comput. Phys. Commun. **269**, 108124 (2021).

[34] R. Zhou and L. Bian, Gravitational wave and electroweak baryogenesis with two Higgs doublet models, Phys. Lett. B **829**, 137105 (2022).

[35] P. Basler, M. Mühlleitner, and J. Müller, Electroweak baryogenesis in the *CP*-violating two-Higgs doublet model, Eur. Phys. J. C **83**, 57 (2023).

[36] K. Enomoto, S. Kanemura, and Y. Mura, Electroweak baryogenesis in aligned two Higgs doublet models, J. High Energy Phys. 01 (2022) 104.

[37] K. Enomoto, S. Kanemura, and Y. Mura, New benchmark scenarios of electroweak baryogenesis in aligned two Higgs double models, J. High Energy Phys. 09 (2022) 121.

[38] D. Gonçalves, A. Kaladharan, and Y. Wu, Gravitational waves, bubble profile, and baryon asymmetry in the complex 2HDM, Phys. Rev. D **108**, 075010 (2023).

[39] J. Baron *et al.* (ACME Collaboration), Order of magnitude smaller limit on the electric dipole moment of the electron, Science **343**, 269 (2014).

[40] L. Bian, T. Liu, and J. Shu, Cancellations between two-loop contributions to the electron electric dipole moment with a *CP*-violating Higgs sector, Phys. Rev. Lett. **115**, 021801 (2015).

[41] K. Fuyuto, W. S. Hou, and E. Senaha, Electroweak baryogenesis driven by extra top Yukawa couplings, Phys. Lett. B **776**, 402 (2018).

[42] T. Modak and E. Senaha, Electroweak baryogenesis via bottom transport, Phys. Rev. D **99**, 115022 (2019).

[43] K. Fuyuto, W. S. Hou, and E. Senaha, Cancellation mechanism for the electron electric dipole moment connected with the baryon asymmetry of the Universe, Phys. Rev. D **101**, 011901 (2020).

[44] T. Modak and E. Senaha, Probing electroweak baryogenesis induced by extra bottom Yukawa coupling via EDMs and collider signatures, J. High Energy Phys. 11 (2020) 025.

[45] S. Kanemura, M. Kubota, and K. Yagyu, Aligned *CP*-violating Higgs sector canceling the electric dipole moment, J. High Energy Phys. 08 (2020) 026.

[46] S. J. Huber, K. Mimasu, and J. M. No, Baryogenesis from spontaneous *CP* violation in the early Universe, Phys. Rev. D **107**, 075042 (2023).
[47] S. Liu and L. Wang, Spontaneous *CP* violation electroweak baryogenesis and gravitational wave through multistep phase transitions, Phys. Rev. D **107**, 115008 (2023).
[48] A. Pich and P. Tuzon, Yukawa Alignment in the two-Higgs-doublet model, Phys. Rev. D **80**, 091702 (2009).
[49] L. Wang and X. F. Han, Status of the aligned two-Higgs-doublet model confronted with the Higgs data, J. High Energy Phys. 04 (2014) 128.
[50] J. Haller, A. Hoecker, R. Kogler, K. Mönig, T. Peiffer, and J. Stelzer, Update of the global electroweak fit and constraints on two-Higgs-doublet models, Eur. Phys. J. C **78**, 675 (2018).
[51] K. Kannike, Vacuum stability conditions from copositivity criteria, Eur. Phys. J. C **72**, 2093 (2012).
[52] J. Dutta, J. Lahiri, C. Li, G. Moortgat-Pick, S. F. Tabira, and J. A. Ziegler, Dark matter phenomenology in 2HDMS in light of the 95 GeV excess, arXiv:2308.05653.
[53] W. Porod, SPheno, A program for calculating supersymmetric spectra, SUSY particle decays and SUSY particle production at $e^+e^-$ colliders, Comput. Phys. Commun. **153**, 275 (2003).
[54] F. Staub, SARAH 4: A tool for (not only SUSY) model builders, Comput. Phys. Commun. **185**, 1773 (2014).
[55] H.-J. He, N. Polonsky, and S. Su, Extra families, Higgs spectrum and oblique corrections, Phys. Rev. D **64**, 053004 (2001).
[56] H. E. Haber and D. ONeil, Basis-independent methods for the two-Higgs-doublet model. III. The *CP*-conserving limit, custodial symmetry, and the oblique parameters S, T, U, Phys. Rev. D **83**, 055017 (2011).
[57] M. Aaboud *et al.* (ATLAS Collaboration), Search for an invisibly decaying Higgs boson or dark matter candidates produced in association with a Z boson in pp collisions at $\sqrt{s} = 13$ TeV with the ATLAS detector, Phys. Lett. B **776**, 318 (2018).
[58] E. Aprile *et al.* (XENON Collaboration), Dark matter search results from a one ton-year exposure of XENON1T, Phys. Rev. Lett. **121**, 111302 (2018).
[59] M. Ackermann *et al.* (Fermi-LAT Collaboration), Searching for dark matter annihilation from Milky Way dwarf spheroidal galaxies with six years of Fermi Large Area Telescope data, Phys. Rev. Lett. **115**, 231301 (2015).
[60] S. R. Coleman and E. J. Weinberg, Radiative corrections as the origin of spontaneous symmetry breaking, Phys. Rev. D **7**, 1888 (1973).
[61] L. Dolan and R. Jackiw, Symmetry behavior at finite temperature, Phys. Rev. D **9**, 3320 (1974).
[62] P. B. Arnold and O. Espinosa, The effective potential and first order phase transitions: Beyond leading-order, Phys. Rev. D **47**, 3546 (1993); **50**, 6662(E) (1994).
[63] R. R. Parwani, Resummation in a hot scalar field theory, Phys. Rev. D **45**, 4695 (1992).
[64] R. Jackiw, Functional evaluation of the effective potential, Phys. Rev. D **9**, 1686 (1974).
[65] H. H. Patel and M. J. Ramsey-Musolf, Baryon washout, electroweak phase transition, and perturbation theory, J. High Energy Phys. 07 (2011) 029.
[66] I. Affleck, Quantum statistical metastability, Phys. Rev. Lett. **46**, 388 (1981).
[67] A. D. Linde, Decay of the false vacuum at finite temperature, Nucl. Phys. **B216**, 421 (1983); **B223**, 544(E) (1983).
[68] A. D. Linde, Fate of the false vacuum at finite temperature: Theory and applications, Phys. Lett. **100B**, 37 (1981).
[69] J. M. Cline, M. Joyce, and K. Kainulainen, Supersymmetric electroweak baryogenesis, J. High Energy Phys. 07 (2000) 018.
[70] L. Fromme and S. J. Huber, Top transport in electroweak baryogenesis, J. High Energy Phys. 03 (2007) 049.
[71] G. F. Giudice and M. E. Shaposhnikov, Strong sphalerons and electroweak baryogenesis, Phys. Lett. B **326**, 118 (1994).
[72] P. Huet and A. E. Nelson, Electroweak baryogenesis in supersymmetric models, Phys. Rev. D **53**, 4578 (1996).
[73] G. D. Moore, Sphaleron rate in the symmetric electroweak phase, Phys. Rev. D **62**, 085011 (2000).
[74] D. Comelli, M. Pietroni, and A. Riotto, Spontaneous CP violation and baryogenesis in the minimal supersymmetric standard model, Nucl. Phys. **B412**, 441 (1994).
[75] G. W. Anderson and L. J. Hall, Electroweak phase transition and baryogenesis, Phys. Rev. D **45**, 2685 (1992).
[76] G. D. Moore, Measuring the broken phase sphaleron rate nonperturbatively, Phys. Rev. D **59**, 014503 (1999).
[77] J. R. Espinosa, B. Gripaios, T. Konstandin, and F. Riva, Electroweak baryogenesis in non-minimal composite Higgs models, J. Cosmol. Astropart. Phys. 01 (2012) 012.
[78] J. McDonald, Electroweak baryogenesis and dark matter via a gauge singlet scalar, Phys. Lett. B **323**, 339 (1994).
[79] C. L. Wainwright, CosmoTransitions: Computing cosmological phase transition temperatures and bubble profiles with multiple fields, Comput. Phys. Commun. **183**, 2006 (2012).
[80] V. Guada, M. Nemevšek, and M. Pintar, FindBounce: Package for multi-field bounce actions, Comput. Phys. Commun. **256**, 107480 (2020).
[81] H. Kudoh, A. Taruya, T. Hiramatsu, and Y. Himemoto, Detecting a gravitational-wave background with next-generation space interferometers, Phys. Rev. D **73**, 064006 (2006).
[82] K. Yagi and N. Seto, Detector configuration of DECIGO/BBO and identification of cosmological neutron-star binaries, Phys. Rev. D **83**, 044011 (2011).